IEEE Access
Multidisciplinary | Rapid Review | Open Access Journal

Received September 10, 2018, accepted October 25, 2018, date of publication October 31, 2018,
date of current version December 3, 2018.

Digital Object Identifier 10.1109/ACCESS.2018.2878940

Stable Propagation of Inhibited Spiking Dynamics in Vertical-Cavity Surface-Emitting Lasers for Neuromorphic Photonic Networks

TAO DENG[1], JOSHUA ROBERTSON[2], ZHENG-MAO WU[1], GUANG-QIONG XIA[1], XIAO-DONG LIN[1], XI TANG[1], ZHI-JING WANG[1], AND ANTONIO HURTADO[2]

[1]School of Physical Science and Technology, Southwest University, Chongqing 400715, China
[2]TIC Centre, SUPA Department of Physics, Institute of Photonics, University of Strathclyde, Glasgow G1 1RD, U.K.

Corresponding authors: Tao Deng (dengt@swu.edu.cn) and Antonio Hurtado (antonio.hurtado@strath.ac.uk)

This work was supported in part by the National Natural Science Foundation of China under Grant 61475127, Grant 61575163, Grant 61775184, Grant 61875167, and Grant 11704316, in part by the Natural Science Foundation of Chongqing City under Grant 2016jcyjA0082, and in part by the Fundamental Research Funds for the Central Universities of China under Grant XDJK2017B012. The work of J. Robertson and A. Hurtado was supported in part by the UK's EPSRC Centre for Doctoral Training, and in part by the US Office of Naval Research Global under Grant ONRG-NICOP-N62909-18-1-2027.

ABSTRACT We investigate experimentally and theoretically the communication of inhibited spiking dynamics between two interlinked photonic neurons based upon the vertical-cavity surface-emitting lasers (VCSELs). We show that the sub-nanosecond speed spiking dynamics fired by a Transmitter-VCSEL (T-VCSEL) can be inhibited under the arrival of suitable external stimuli and that the inhibited spiking behaviors are propagated into another Receiver-VCSEL (R-VCSEL). Both VCSELs exhibit analogous inhibited spiking dynamics in response to stimuli with different temporal durations and strength. In addition, a very good agreement is found between theoretical simulations and experiments. These results offer greater prospects for future networks of VCSEL-based photonic neurons for neuromorphic computing platforms.

INDEX TERMS Vertical-cavity surface-emitting lasers (VCSELs), unidirectional coupling, inhibited spiking dynamics, stable propagation.

I. INTRODUCTION

Spiking Neural Networks (SNNs), referred to as the third generation of neural networks, possess some unique advantages such as the bandwidth efficiency of analog processing and the noise robustness of digital computation, and offer high potential to solve highly complex computational problems, e.g. pattern recognition, decision-making, optimization and learning, etc. [1]. The development of SNNs greatly prompts the advancement of information processing techniques and a number of large-scale SNNs based in electronic techniques have been developed. For example, IBM's TrueNorth that integrates a million spiking-neurons [2], Neurogrid at Stanford University [3], HICANN at University of Heidelberg [4] and the Neuromorphic chip at University of Manchester [5]. However, these electronic SNNs models experience drawbacks (e.g. limited bandwidths, cross-talk, reduced communication links, high power consumption) affecting their performance and resulting in longer operation timescales [6].

Recently, new photonic approaches for spiking neuron models based upon photonic techniques have been proposed. These can yield ultrafast spiking responses, up to 9 orders of magnitude faster than biological neurons. These included approaches based on semiconductor optical amplifiers [7], [8], fiber lasers with graphene [9], [10], photonic crystal cavities [11], [12], and semiconductor lasers (SLs) [13]–[15]. These photonic techniques offer great promise to break through the electronic bandwidth limitation whilst also allowing for reduced energy requirements during operation. Also recently, photonic functionalities for such systems, such as all-optical digital-to-spike conversion have started to appear [16]. Hence, these photonic approaches of neuronal models offer prospects for novel neuromorphic photonic systems in information processing and computing.

Among these, SL-based photonic neuron models have dominated and recently, laser-based spiking photonic neuron models have been demonstrated with multiple designs, including semiconductor micro-ring lasers [17], [18], laser diodes driven by resonant tunneling diode photodetectors [19], optically injected micro-disk lasers [20], Quantum Dot SLs [21], [22], devices with saturable absorbing

sections [23], semiconductor lasers with external feedback [24], micropillar lasers in conjunction with a saturable absorber (SA) [25] and VCSELs [26]–[31]. We have focused on the latter given the unique advantages of these devices, such as low energy consumption, easy integration into 2D arrays, high coupling efficiency to optical fibers, low manufacturing costs, and have produced early reports on VCSEL-based photonic neuronal models [26]–[31]. As for biological neurons, these react to incoming stimuli by producing spike firing signals. However, in neurons the inhibition of spiking responses under arriving perturbations also plays an important role in brain activity [32]–[34]. Hence the achievement of spiking inhibitory responses with photonic neuronal models has also attracted extensive investigation [35], [36].

The approaches mentioned above mostly focus on the generation and inhibition of spiking regimes in a single photonic neuron. However, the interconnection of different biological neurons is necessary for some important functional implementation. For example, synchronization of neural activity in brain has becomes the key of cognitive activity. Obviously, different topological network schemes consisting of two or more photonic neurons are strictly necessary for future information processing scenarios. Nonetheless, efforts on interconnected systems are still limited to a few works having focused mainly on planar semiconductor laser designs [37]–[39]. Very recently, network schemes of spiking VCSEL-based photonic neurons have undergone preliminarily investigation and the communication of spike firing patterns between two interconnected VCSEL neurons has been analyzed numerically [31] and experimentally [40]. In [31], different connection topologies including unidirectional coupling and mutual coupling between two VCSELs are discussed and the propagation of fired spiking dynamics between two interconnected VCSELs is theoretically demonstrated [31]. Very recently, we demonstrated experimentally the successful communication of controllable spiking patterns between two interconnected VCSEL photonic neurons [40].

These early demonstrations also pave the way to the development of inhibitory photonic neural network models, where spiking inhibited responses can be successfully propagated between interlinked VCSEL-based photonic neuronal models for future neuromorphic photonic networks enabling both excitatory and inhibitory spiking responses. Different with the fired spiking propagation in literatures [31] and [40], this paper focuses on this aspect to demonstrate experimentally and numerically the stable propagation of inhibited spiking information at sub-nanosecond speeds between two unidirectionally coupled VCSEL-based photonic neurons. We shows that controlled inhibition regimes of spiking dynamics in a Transmitter-VCSEL (T-VCSEL), induced by an external perturbation, can be successfully propagated to a Receiver-VCSEL (R-VCSEL). Importantly, our results are obtained at the important telecom wavelength of 1300 nm, making our approach fully compatible with current fibre-optic data communication systems. Additionally, a theoretical model analyzing the spike propagation characteristics of such a system has also been developed with good agreement between simulated and experimentally achieved results.

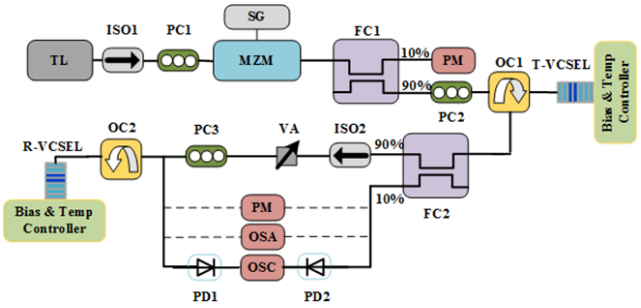

FIGURE 1. Experimental setup. TL: tunable laser; T-VCSEL: transmitter-VCSEL; R-VCSEL: receiver-VCSEL; ISO: isolator; PC: polarization controller; MZM: Mach-Zehnder Modulator; SG: signal generator; FC: fiber coupler; PM: power meter; OC: optical circulator; VA: variable attenuator; OSA: optical spectrum analyzer; OSC: oscilloscope.

II. EXPERIMENTAL SETUP

The schematic diagram of our experimental setup is shown in Fig. 1. Two commercial 1300 nm VCSELs (Raycan) are used as the photonic neuronal models. The bias current and temperature of the VCSELs are controlled by high accuracy laser drivers (Newport, LDDM-5005) and temperature controllers (Profile, TED 200). The continuous light from a tunable laser (TL) is modulated by a Mach-Zehnder modulator (MZM, JDSU MOD-9189) after passing through an isolator (ISO1) and a polarization controller (PC1). Temporal perturbations, in the form of short power raises are encoded in the continuous light from the TL using the MZM and a signal generator (SG). The perturbed signal is injected into the transmitter VCSEL (T-VCSEL) through a 90:10 fiber coupler (FC1), a second polarization controller (PC2) and an optical circulator (OC1). The output from T-VCSEL is divided into two parts by a 90:10 fiber coupler (FC2). The 90% output port from FC2 is injected into the receiver VCSEL (R-VCSEL) after passing through a second isolator (ISO2), a variable attenuator (VA), a polarization controller (PC3) and an optical circulator (OC2). The remaining 10% of the signal from FC2 is sent into the detection system. A high-speed amplified photodetector (PD2, Thorlabs PDA8GS, 9.5 GHz bandwidth) and a digital real-time oscilloscope (OSC, Agilent DSO 81304B, 13 GHz bandwidth) are utilized to capture the time series, an optical spectrum analyzer (OSA, Anritsu MS9710C) is used to analyze the optical spectrum distribution, and a power meter (PM) is used to monitor the injection power into the two VCSELs. Similarly, the output from the R-VCSEL is sent to the detection system via OC2 and another high-speed amplified photodetector (PD1). During the experiment, the temperatures of both VCSELs were respectively kept constant at 300 K (T-VCSEL) and 292 K (R-VCSEL) except additional description. Under this condition, the threshold currents for both

VCSELs were measured equal to $I_{th,T} = 0.60$mA and $I_{th,R} = 0.61$ mA, respectively.

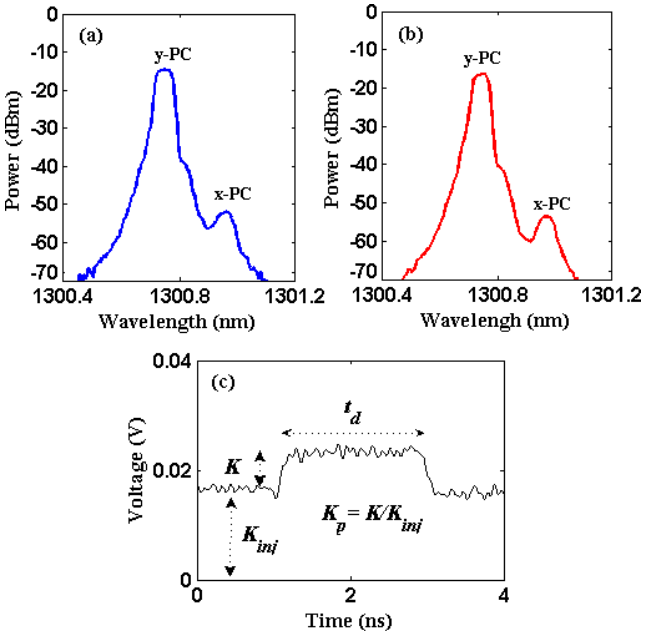

FIGURE 2. Experimentally measured optical spectra of the T-VCSEL (a), R-VCSEL (b) and a typical external perturbation (c).

III. RESULTS AND DISCUSSION

Figures 2(a)-2(b) record the experimentally measured optical spectra of the two free-running VCSELs used in the experiment, with T-VCSEL and R-VCSEL biased at 1.5 mA ($\sim$2.5 $I_{th,T}$) and 1.5 mA ($\sim$2.5 $I_{th,R}$) respectively. The main lasing and subsidiary modes of the devices are referred to as the parallel polarization (y-PC) and orthogonal polarization (x-PC) components of the fundamental transverse mode, respectively. Fig. 2(c) shows a typical injected signal with an encoded stimulus (or perturbation) into T-VCSEL. The encoded stimulus is characterized by a constant injection level K_{inj} and a controllable strength K, temporal duration t_d and repetition rate $f_{rep} = 15$ MHz. K_p is defined as the ratio between perturbation pulse strength and constant injection level ($K_p = K/K_{inj}$). In our experimental setup, the time delay between the T-VCSEL and R-VCSEL was approximately equal to 62 ns.

Figure 3(a) plots the real-time series at the output of T-VCSEL subject to the injection of the signal in the inset at the top of Fig. 3(a). Here, the externally injected signals (with encoded perturbations) are set with orthogonal polarization (to that of the main lasing mode of the devices) and injected into the orthogonal polarization mode of T-VCSEL. The constant injection power was equal to 28.56 μW, and the temporal duration t_d and strength K_p of the added perturbation signal were equal to 2.0 ns and 0.495, respectively. The frequency detuning Δf between the externally injected signal and T- VCSEL was $\Delta f_{IT} = f_{inj} - f_{Tx} = -3.68$ GHz, where f_{inj} and f_{Tx} correspond to the frequencies of the external injection

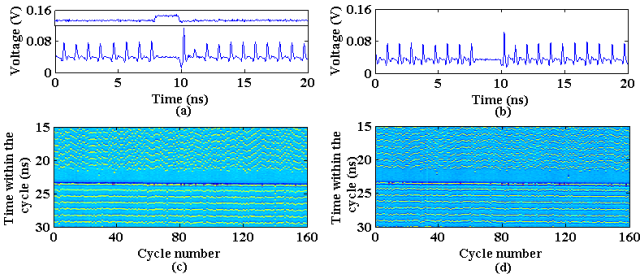

FIGURE 3. (a-b) Time series measured at the output of T-VCSEL (a) and R-VCSEL (b). The external signal (stimulus) injected into T-VCSEL, shown in the inset at the top of (a), was characterized by a constant injection level of $K_{inj} = 28.56\mu$W, temporal duration of $t_d = 2.0$ ns and $K_p = 0.495$. (c-d) Corresponding temporal maps obtained from the captured time-series from T-VCSELs (c) and R-VCSELs (d) show their responses to the arrival of 160 consecutive external perturbations into T-VCSEL.

and that of the orthogonal polarization mode of the T-VCSEL. From Fig. 3(a), it can be seen that T-VCSEL operates at a continuous spiking regime under a constant injection level. Once the perturbation arrives, it is forced into an injection-locking state and the spikes are suppressed due to the sudden increase in the injection level. When the perturbation is removed, the inhibited response disappears and the laser switches back to a tonic spiking regime. It should be pointed out that there is a $\sim$ 62 ns time delay between the T-VCSEL and R-VCSEL, which corresponds to the flight time between the two lasers. For comparison purposes, the output time series of R-VCSEL were shifted to plot them in the same time-scales as those of T-VCSEL. Additionally, to verify the validity and stability of this response, Fig. 3 (c) shows the temporal map of superimposed time series from the T-VCSEL, where the time interval between two consecutive events ($T_{rep} = 1/f_{rep}$) is used as the folding parameter, and the T-VCSEL's response to the arrival of 160 identical perturbations is observed. The color coding in the map indicates increasing intensity from blue to red. Red/Yellow colors correspond to high intensity spikes, while blue dotes denote a constant intensity and darker blue dots indicate power drops below the steady state. Fig. 3(c) clearly shows the reproducibility of the spiking inhibition response in T-VCSEL to all incoming perturbations. Subsequently, all output light from T-VCSEL is orthogonally injected into the subsidiary orthogonally-polarized mode of R-VCSEL and the corresponding responses are shown in Fig. 3(b). Here, the constant injection power is 60.11 μW, and the detuning frequency (Δf_{TR}) between the two lasers is set to $\Delta f_{TR} = f_{Tx} - f_{Rx} = -2.76$ GHz, where f_{Rx} corresponds to the frequency of the orthogonal polarization mode of R-VCSEL and the frequency detuning is achieved by adjusting the temperature of R-VCSEL. Under continuous injection from T-VCSEL, the response of R-VCSEL repeatedly goes from the spiking regime to the injection-locking regime, then back to the spiking regime. The corresponding temporal map, captured at the output of R-VCSEL in response to 160 consecutive perturbations from T-VCSEL, is shown in Fig. 3(d). It should be pointed out that the difference of phase noise before and

after perturbation observed in the maps of Figs. 3(c)-3(d) is simply due to a data processing issue. In fact, a small mismatch between the actual inhibition-event interval and the folding time used to produce the maps can induce the drift of the dynamics. For comparison, we suitably shifted the time sequences through fixing the first spike fired after removing the perturbation. Moreover, the inherent instability of this system also strengthen to the difference. These results therefore show that a reproducible spiking inhibition behavior, with a consistent response to consecutive external perturbations, can be obtained for the T-VCSEL and can be in turn propagated to R-VCSEL, hence demonstrating the achievement the communication of inhibitory neuronal responses at sub-nanosecond speed rates in a network of two VCSEL-based photonic neurons.

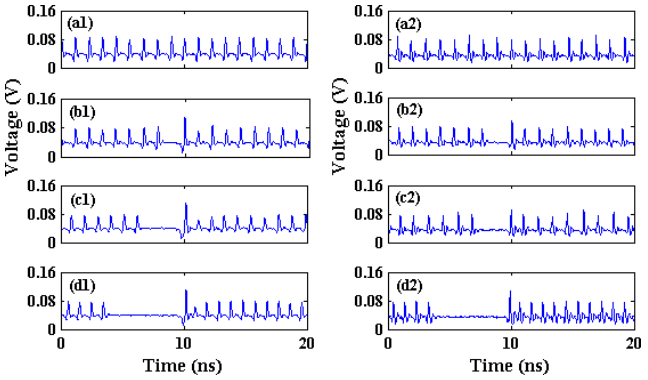

FIGURE 4. Experimentally measured time series of T-VCSEL and R-VCSEL in response to perturbations with different temporal duration t_d: (a) 0 ns, (b) 1.35 ns, (c) 2.50 ns and (d) 5.80 ns and with constant perturbation strength $K_P = 0.417$.

To further explore the propagation properties of the spiking inhibition behavior between two interconnected VCSEL neurons, Fig. 4 gives the time series from T-VCSEL and R-VCSEL for the injection of external signals with increasing perturbation duration t_d from 0 ns to 5.80 ns and constant perturbation strength $K_p = 0.417$. When no perturbations arrive ($t_d = 0$ ns), Fig. 4 (a1) shows that T-VCSEL operates in a spiking regime where consecutive spikes with sub-nanosecond time intervals are fired. When increasing t_d from 1.35 ns (Fig. 4(b1)) to 2.50 ns (Fig. 4(c1)), and 5.80 ns (Fig. 4(d1)), the spiking dynamics from T-VCSEL are entirely suppressed during the perturbation period since T-VCSEL is forced from the spiking into the injection-locking regime. Fig. 4 thus shows that the window of inhibited spiking dynamics can be controlled by adjusting experimentally the perturbation duration t_d. The responses of R-VCSEL are also provided in Figs. 4(a2)-(d2), showing that the inhibitory spiking dynamics with different and controlled temporal length from T-VCSEL can be successfully communicated to R-VCSEL. It should be highlighted that the responses observed from both T- and R-VCSELs are analogous with only slight differences caused by noise and inherent instabilities in our experimental system.

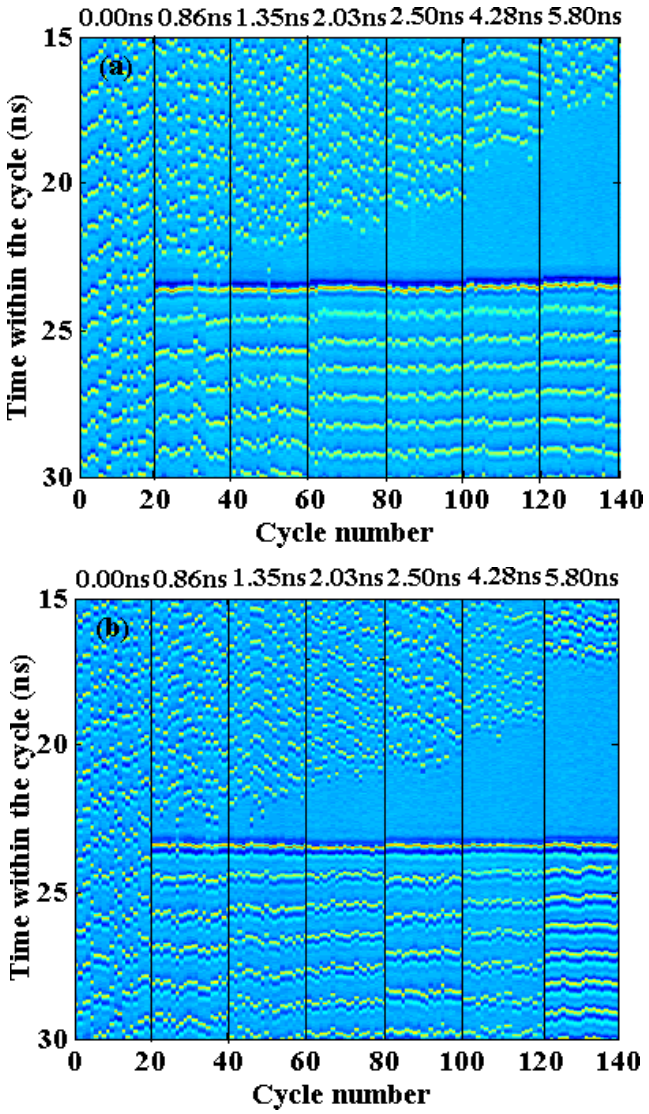

FIGURE 5. Temporal maps of the T-VCSEL (a) and R-VCSEL (b) outputs plotting the response to 20 consecutive perturbations for 7 different values of perturbation temporal duration, t_d, as indicated. All other parameters are the same as in Fig. 4.

Figure 5 shows in turn temporal maps built from the time-series at the output of the T- and R-VCSELs. The two maps in Fig. 5 consist of 7 segments, each one of them plotting 20 superimposed time series for a different considered value of t_d (from 0 to 5.80 ns, as indicated). All other parameters are the same as in Fig. 4. From the maps in Fig. 5, it can be seen that the controllable and repeatable inhibition pattern of spiking dynamics can be obtained from T-VCSEL by adjusting t_d from 0 ns to 5.80 ns. Moreover, the stable propagation of inhibited spiking dynamics between T-VCSEL and R-VCSEL is also achieved.

Figure 6 shows the time series at the output of T-VCSEL and R-VCSEL for external perturbations with fixed temporal duration of $t_d = 5.8$ ns and varying strength (K_p) going from 0 to 0.42. The constant power levels injected to each of the two VCSELs were equal to 46.10 μW and 52.28 μW, respectively. The frequency detunings set for the

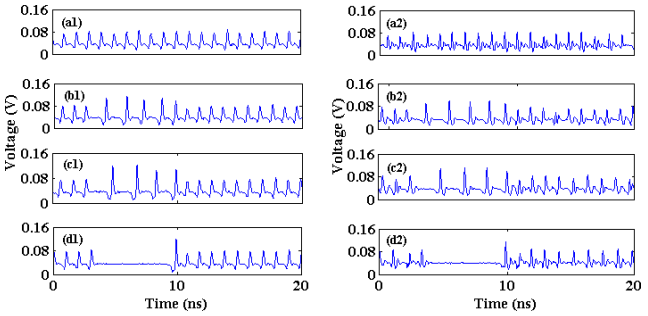

FIGURE 6. Time series of T-VCSEL and R-VCSEL in response to perturbations of increasing strength (K_P): (a) 0, (b) 0.29, (c) 0.32 and (d) 0.42, at constant $t_d = 5.8$ ns.

two VCSELs were respectively equal to −3.55 GHz and −2.84 GHz. When increasing the perturbation strength to $K_p = 0.29$ and 0.32, spikes with longer inter-spiking period are initially fired, as shown in Figs. 6(b) and 6(c). Further increasing the perturbation to $K_p = 0.42$, causes the spikes during the perturbation window to be entirely suppressed, as shown in Fig. 6(d). These results therefore demonstrate the existence of a perturbation strength threshold, above which, firing spikes are entirely suppressed for the duration of the perturbation window [36].

IV. THEORY MODEL AND RESULTS

Based on the spin-flip model (SFM), after taking into account the influence of optical injection, the modified rate equations of the VCSELs can be described by [40], [41]:

$$\begin{aligned}\frac{dE^{T}_{x,y}}{dt} &= -\left(k^{T} \pm \gamma^{T}_{a}\right) E^{T}_{x,y} - i\left(k^{T}\alpha^{T} \pm \gamma^{T}_{p}\right) E^{T}_{x,y} \\ &\quad + k^{T}\left(1 + i\alpha^{T}\right)\left(N^{T}E^{T}_{x,y} \pm in^{T}E^{T}_{y,x}\right) \\ &\quad + \eta_1 E_{injx,injy}(t)\, e^{i\Delta\omega_{x,y}t} + F^{T}_{x,y} \qquad (1)\end{aligned}$$

$$\begin{aligned}\frac{dE^{R}_{x,y}}{dt} &= -\left(k^{R} \pm \gamma^{R}_{a}\right) E^{R}_{x,y} - i\left(k^{R}\alpha^{R} \pm \gamma^{R}_{p}\right) E^{R}_{x,y} \\ &\quad + k^{R}\left(1 + i\alpha^{R}\right)\left(N^{R}E^{R}_{x,y} \pm in^{R}E^{R}_{y,x}\right) \\ &\quad + \eta_2 E^{T}_{x,y}(t)\, e^{-i\omega^{T}_{x,y}\tau + i\Delta\omega_{TR}t} + F^{R}_{x,y} \qquad (2)\end{aligned}$$

$$\begin{aligned}\frac{dN^{T,R}}{dt} &= -\gamma^{T,R}_{e}[N^{T,R}\left(1 + \left|E^{T,R}_{x}\right|^{2} + \left|E^{T,R}_{y}\right|^{2}\right) - \mu^{T,R} \\ &\quad + in^{T,R}(E^{T,R}_{y}E^{T,R*}_{x} - E^{T,R}_{x}E^{T,R*}_{y})] \qquad (3)\end{aligned}$$

$$\begin{aligned}\frac{dn^{T,R}}{dt} &= -\gamma^{T,R}_{s}n^{T,R} - \gamma^{T,R}_{e}[n^{T,R}\left(\left|E^{T,R}_{x}\right|^{2} + \left|E^{T,R}_{y}\right|^{2}\right) \\ &\quad + iN^{T,R}(E^{T,R}_{y}E^{T,R*}_{x} - E^{T,R}_{x}E^{T,R*}_{y})] \qquad (4)\end{aligned}$$

where superscripts T and R stand for T-VCSEL and R-VCSEL, respectively, and subscripts x and y stand for the X- orthogonal and Y- parallel polarization components. E is the slowly varying complex amplitude. E_{injx} (E_{injy}) represents the injected light field into the X- (Y-) polarization components. N is the total population inversion between the conduction and valence bands and n is the difference between the population inversions for spin-up and spin-down radiation channels. k is the decay rate of the electric field in the VCSEL cavity. α is the linewidth enhancement factor. γ_e is the decay rate of the total population inversion and γ_s is the spin-flip relaxation rate. γ_a and γ_p are respectively the linear dichroism and the cavity birefringence rate.τ is the optical flight time from T-VCSEL to R-VCSEL and μ is the normalized injection current. $\Delta\omega_x$ ($\Delta\omega_y$) indicates the detuning between the angular frequency of the x-polarized (or y-polarized) externally injected light ω_{injx} (ω_{injy}) and a reference angular frequency situated at the middle point between those of the VCSEL's X- and Y- polarization components, *i.e.*$\Delta\omega_x = \omega_{injx} - (\omega^{T}_{x} + \omega^{T}_{y})/2$ ($\Delta\omega_y = \omega_{injy} - (\omega^{T}_{x} + \omega^{T}_{y})/2$). $\Delta\omega_{TR}$ refers to the frequency detuning between the frequencies of the two VCSELs: T-VCSEL (ω^{T}) and R-VCSEL (ω^{R}), *i.e.*$\Delta\omega_{TR} = \omega^{T} - \omega^{R}$. η_1 and η_2 are the injected coupling coefficients for the T-VCSEL and R-VCSEL, respectively. F corresponds to the spontaneous emission noise determined by:

$$\begin{aligned}F^{T,R}_{x} &= \sqrt{\frac{\beta^{T,R}_{sp}\gamma^{T,R}_{e}}{2}}\left(\sqrt{N^{T,R} + n^{T,R}}\,\xi^{T,R}_{1}\right. \\ &\quad \left. + \sqrt{N^{T,R} - n^{T,R}}\,\xi^{T,R}_{2}\right) \qquad (5)\end{aligned}$$

$$\begin{aligned}F^{T,R}_{y} &= -i\sqrt{\frac{\beta^{T,R}_{sp}\gamma^{T,R}_{e}}{2}}\left(\sqrt{N^{T,R} + n^{T,R}}\,\xi^{T,R}_{1}\right. \\ &\quad \left. - \sqrt{N^{T,R} - n^{T,R}}\,\xi^{T,R}_{2}\right) \qquad (6)\end{aligned}$$

where β_{sp} is the spontaneous emission factor, ξ_1 and ξ_2 are independent complex Gaussian white noise sources with zero mean and unit variance. The rate equations (1) - (6) can be numerically solved using the fourth-order Runge-Kutta method. For simplicity, during calculations, the normalized injection current and all the internal parameters for T-VCSEL and R-VCSEL are assumed to be identical and the parameters used are as follows [40]–[42]: $\alpha = 2$, $k = 250$ ns^{-1}, $\gamma_e = 0.5$ ns^{-1}, $\gamma_s = 10^5$ ns^{-1}, $\gamma_a = 2$ ns^{-1}, $\beta_{sp} = 10^{-6}$, $\gamma_p = 128$ ns^{-1}, $\tau = 62$ ns, $\mu = 1.7$, $\eta_1 = 125$ ns^{-1}, $\eta_2 = 100$ ns^{-1} and the central frequency of VCSEL is 1.45×10^{15} rad/s (corresponding to the central wavelength of the VCSEL at 1300 nm).

Figures 7(a)-7(h) plot the numerically calculated time series from the interconnected T-VCSEL and R-VCSEL when the former is subject to the injection of external perturbations of fixed strength ($K_p = 0.36$) and varied duration t_d (from 0 to 4.5 ns). For the case without any perturbations, spikes, at sub-ns intervals, are tonically fired by T-VCSEL and these spiking dynamics are propagated to R-VCSEL, as shown in Figs. 7(a1)-7(a2). As a result, encoded spiking communication between the two interconnected VCSELs is achieved. By increasing the perturbation duration, the spikes in T-VCSEL's output are suppressed for the entirety of the perturbation window (see Figs. 7(b1)-7(h1)) with a similar response obtained from R-VCSEL, as shown in Figs. 7(a2)-7(h2). Further, Figs. 7(i)-7(j) plot the corresponding temporal maps for the T- and R-VCSEL outputs in response to 20 consecutive perturbations for 8 different

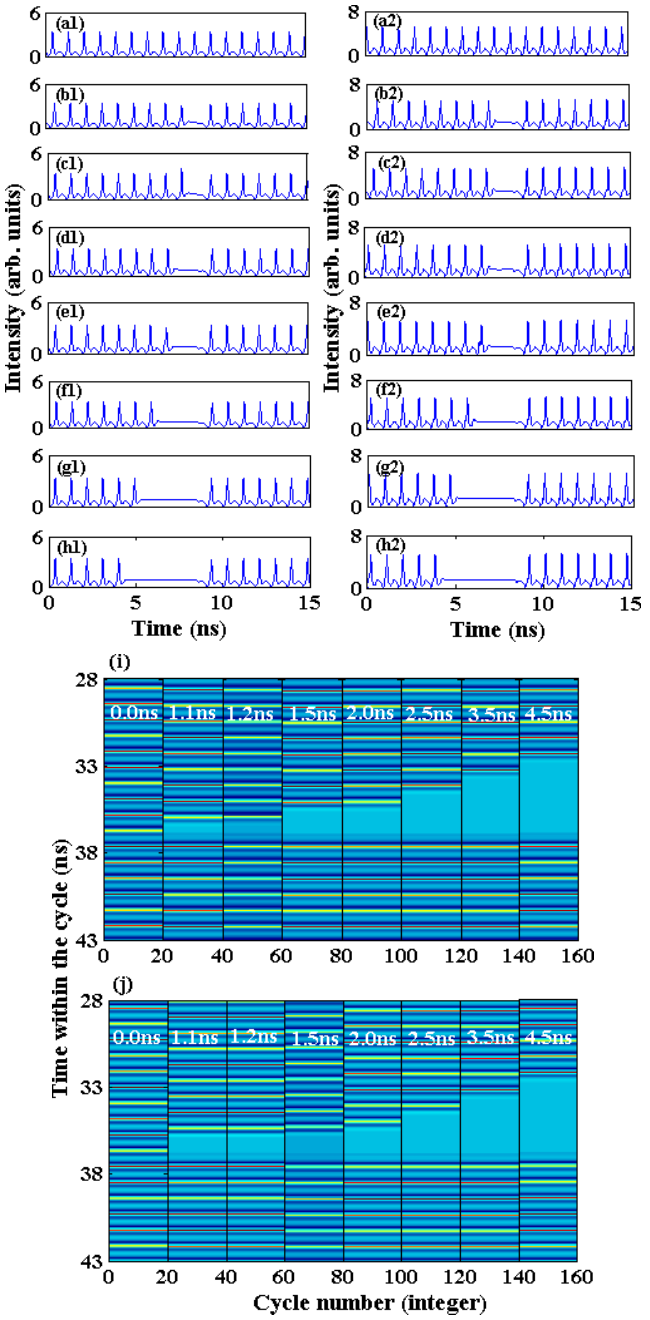

FIGURE 7. Numerically calculated time series of T-VCSEL and R-VCSEL in response to perturbations with different t_d (a) 0 ns, (b) 1.1 ns, (c) 1.2 ns, (d) 1.5 ns, (e) 2.0 ns, (f) 2.5 ns, (g) 3.5 ns and (h) 4.5 ns, at constant $K_p = 0.36$, and corresponding temporal maps of the T-VCSEL (i) and R-VCSEL (j).

perturbation durations t_d (from 0 to 4.5 ns). The color coding scheme is the same as that in Fig. 5. These maps clearly show that the windows of inhibitory spiking regimes in T-VCSEL can be tuned by adjusting the perturbations duration and can be propagated from T-VCSEL to R-VCSEL. These calculated results show excellent agreement with our experimental findings shown in Fig. 5.

Figures 8(a)-8(d) show the numerically calculated time series for T-VCSEL and R-VCSEL, where the former is subject to external injection with encoded perturbations

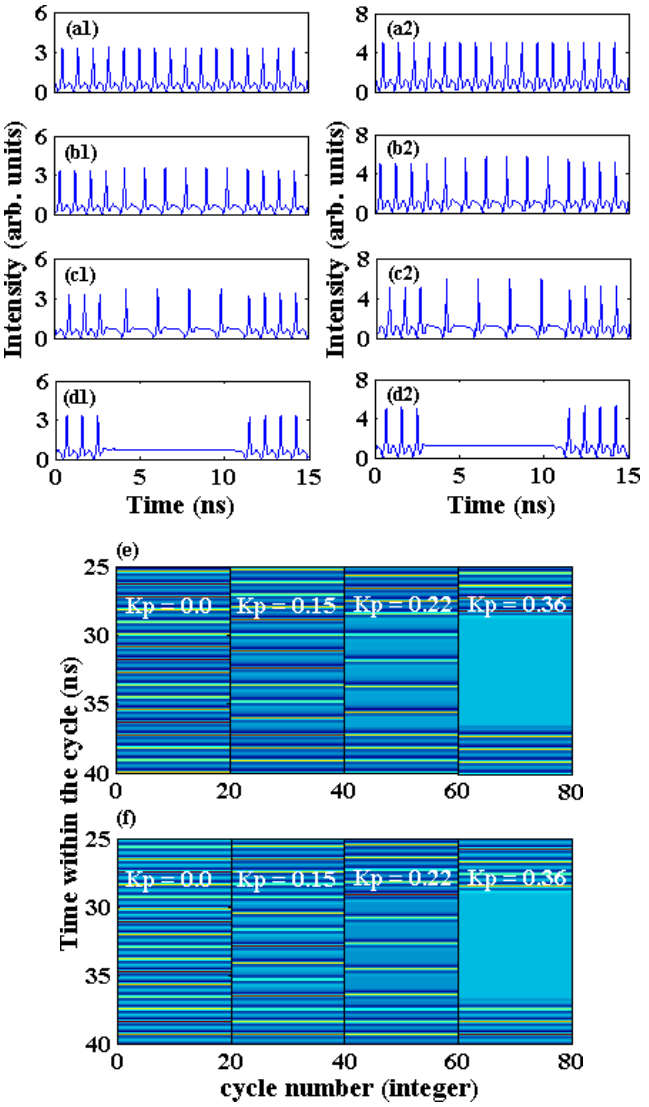

FIGURE 8. Numerically calculated time series of T-VCSEL and R-VCSEL in response to perturbations with different strength K_P (a) 0.0, (b) 0.15, (c) 0.22 and (d) 0.36, and constant temporal duration $t_d = 8$ ns, and corresponding temporal maps of the T-VCSEL (e) and R-VCSEL (f).

with constant temporal duration, t_d of 8 ns and increasing strength, K_p (0 to 0.36). From Figs. 8(a)-8(d) it can be seen that for relatively low perturbation strengths, spikes with increasingly longer inter-spiking intervals are fired for the entirety of the perturbation. When the perturbation strength is increased above a certain threshold level, the spikes are completely suppressed as long as the perturbation is present. This behavior can be explained as follows, the increasing injection strength pushes the VCSEL to a longer resonance wavelength, decreasing the wavelength detuning between the externally injected signal and the laser oscillator, and as a result the spiking repetition frequency increases the spiking period. When the injection strength is increased to a higher level, sufficient enough to force the laser into the injection-locking state, the spikes during the perturbation window are fully suppressed. Moreover, these dynamical behaviors from T-VCSEL are successfully transmitted to

R-VCSEL, as shown in Figs. 8(a2)-8(d2). Additionally, the temporal maps corresponding to the time series in Figs. 8(a)-8(d) are shown in Figs. 8(e)-8(f). The temporal maps show the response of the T- and R-VCSELs to 20 consecutive perturbations for each of the values of perturbation strength, K_p (from 0.0 to 0.36) considered, where the color coding scheme is the same to that in Fig. 5. Again, very good agreement with the experimental findings is observed.

V. CONCLUSIONS

In summary, we investigate a photonic spiking neural network based on two interconnected 1300 nm VCSEL-based photonic neuronal models and we demonstrate the communication of inhibitory spiking dynamical regimes in such a system. When an external light signal with encoded short temporal perturbations is injected into the first VCSEL-neuron (T-VCSEL), the spiking inhibition regime obtained at the output of T-VCSEL can be effectively controlled by adjusting the perturbations' temporal duration and strength. The spiking inhibited responses from the T-VCSEL can then be transmitted into the second VCSEL neuron (R-VCSEL) where similar spiking dynamics are produced. Our results show that the spiking inhibition behavior obtained from the VCSEL-photonic neuronal models subject to external incoming perturbation is analogous to that of inhibitory biological neurons in the brain, but at a much faster timescales (sub-nanosecond speeds compared to millisecond timescales in biological neurons). The successful demonstration of stable communication of spiking inhibition dynamics between two interconnected VCSEL photonic neurons offers great potential for future, brain-inspired photonic neural networks, combining both excitatory and inhibitory functionalities for use in novel ultrafast neuromorphic computing systems.

REFERENCES

[1] P. R. Prucnal and B. J. Shastri, *Neuromorphic Photonics*. Boca Raton, FL, USA: CRC Press, 2017.

[2] J. Hsu, "IBM's new brain," *IEEE Spectrum*, vol. 51, no. 10, pp. 17–19, Oct. 2014.

[3] B. V. Benjamin *et al.*, "Neurogrid: A mixed-analog-digital multichip system for large-scale neural simulations," *Proc. IEEE*, vol. 102, no. 5, pp. 699–716, May 2014.

[4] J. Schemmel, D. Briiderle, A. Griibl, M. Hock, K. Meier, and S. Millner, "A wafer-scale neuromorphic hardware system for large-scale neural modeling," in *Proc. IEEE Int. Symp. Circuits Syst.*, May/Jun. 2010, pp. 1947–1950.

[5] M. M. Khan *et al.*, "SpiNNaker: Mapping neural networks onto a massively-parallel chip multiprocessor," in *Proc. IEEE Int. Joint Conf. Neural Netw. (IJCNN)*, Jun. 2008, pp. 2849–2856.

[6] P. R. Prucnal, B. J. Shastri, T. F. de Lima, M. A. Nahmias, and A. N. Tait, "Recent progress in semiconductor excitable lasers for photonic spike processing," *Adv. Opt. Photon.*, vol. 8, no. 2, pp. 228–299, Jun. 2016.

[7] M. P. Fok, Y. Tian, D. Rosenbluth, and P. R. Prucnal, "Asynchronous spiking photonic neuron for lightwave neuromorphic signal processing," *Opt. Lett.*, vol. 37, no. 16, pp. 3309–3311, Aug. 2012.

[8] K. Kravtsov, M. P. Fok, D. Rosenbluth, and P. R. Prucnal, "Ultrafast all-optical implementation of a leaky integrate-and-fire neuron," *Opt. Express*, vol. 19, no. 3, pp. 2133–2147, Jan. 2011.

[9] B. J. Shastri, M. A. Nahmias, A. N. Tait, B. Wu, and P. R. Prucnal, "SIMPEL: Circuit model for photonic spike processing laser neurons," *Opt. Express*, vol. 23, no. 6, pp. 8029–8044, Mar. 2015.

[10] B. J. Shastri, M. A. Nahmias, A. N. Tait, A. W. Rodriguez, B. Wu, and P. R. Prucnal, "Spike processing with a graphene excitable laser," *Sci. Rep.*, vol. 6, p. 19126, Jan. 2016.

[11] A. M. Yacomotti *et al.*, "Fast thermo-optical excitability in a two-dimensional photonic crystal," *Phys. Rev. Lett.*, vol. 97, no. 14, pp. 143904-1–143904-4, Oct. 2006.

[12] M. Brunstein, A. M. Yacomotti, I. Sagnes, F. Raineri, L. Bigot, and A. Levenson, "Excitability and self-pulsing in a photonic crystal nanocavity," *Phys. Rev. A, Gen. Phys.*, vol. 85, no. 3, pp. 031803-1–031803-5, Mar. 2012.

[13] F. Selmi *et al.*, "Spike latency and response properties of an excitable micropillar laser," *Phys. Rev. E, Stat. Phys. Plasmas Fluids Relat. Interdiscip. Top.*, vol. 94, no. 4, pp. 042219-1–042219-9, Oct. 2016.

[14] B. Garbin, J. Javaloyes, G. Tissoni, and S. Barland, "Topological solitons as addressable phase bits in a driven laser," *Nature Commun.*, vol. 6, Jan. 2015, Art. no. 5915.

[15] J. Javaloyes, T. Ackemann, and A. Hurtado, "Arrest of domain coarsening via antiperiodic regimes in delay systems," *Phys. Rev. Lett.*, vol. 115, no. 20, pp. 203901-1–203901-6, Nov. 2015.

[16] P. Y. Ma, B. J. Shastri, T. F. de Lima, A. N. Tait, M. A. Nahmias, and P. R. Prucnal, "All-optical digital-to-spike conversion using a graphene excitable laser," *Opt. Express*, vol. 25, no. 26, pp. 33504–33513, Dec. 2017.

[17] L. Gelens *et al.*, "Excitability in semiconductor microring lasers: Experimental and theoretical pulse characterization," *Phys. Rev. A, Gen. Phys.*, vol. 82, no. 6, pp. 063841-1–063841-9, Dec. 2010.

[18] W. Coomans, L. Gelens, S. Beri, J. Danckaert, and G. Van der Sande, "Solitary and coupled semiconductor ring lasers as optical spiking neurons," *Phys. Rev. E, Stat. Phys. Plasmas Fluids Relat. Interdiscip. Top.*, vol. 84, no. 3, p. 036209, 2011.

[19] B. Romeira, J. Javaloyes, C. N. Ironside, J. M. L. Figueiredo, S. Balle, and O. Piro, "Excitability and optical pulse generation in semiconductor lasers driven by resonant tunneling diode photo-detectors," *Opt. Express*, vol. 21, no. 18, pp. 20931–20940, Sep. 2013.

[20] K. Alexander, T. Van Vaerenbergh, M. Fiers, P. Mechet, J. Dambre, and P. Bienstman, "Excitability in optically injected microdisk lasers with phase controlled excitatory and inhibitory response," *Opt. Express*, vol. 21, no. 22, pp. 26182–26191, Nov. 2013.

[21] J. Robertson, T. Ackemann, L. F. Lester, and A. Hurtado, "Externally-triggered activation and inhibition of optical pulsating regimes in quantum-dot mode-locked lasers," *Sci. Rep.*, vol. 8, Aug. 2018, Art. no. 12515.

[22] C. Mesaritakis, A. Kapsalis, A. Bogris, and D. Syvridis, "Artificial neuron based on integrated semiconductor quantum dot mode-locked lasers," *Sci. Rep.*, vol. 6, Dec. 2016, Art. no. 39317.

[23] S. Barbay, R. Kuszelewicz, and A. M. Yacomotti, "Excitability in a semiconductor laser with saturable absorber," *Opt. Lett.*, vol. 36, no. 23, pp. 4476–4478, Dec. 2011.

[24] A. Aragoneses, S. Perrone, T. Sorrentino, M. C. Torrent, and C. Masoller, "Unveiling the complex organization of recurrent patterns in spiking dynamical systems," *Sci. Rep.*, vol. 4, Apr. 2014, Art. no. 4696.

[25] F. Selmi, R. Braive, G. Beaudoin, I. Sagnes, R. Kuszelewicz, and S. Barbay, "Relative refractory period in an excitable semiconductor laser," *Phys. Rev. Lett.*, vol. 112, no. 18, p. 183902, May 2014.

[26] A. Hurtado, K. Schires, I. D. Henning, and M. J. Adams, "Investigation of vertical cavity surface emitting laser dynamics for neuromorphic photonic systems," *Appl. Phys. Lett.*, vol. 100, no. 10, pp. 103703-1–103703-4, Mar. 2012.

[27] A. Hurtado and J. Javaloyes, "Controllable spiking patterns in long-wavelength vertical cavity surface emitting lasers for neuromorphic photonics systems," *Appl. Phys. Lett.*, vol. 107, no. 24, pp. 241103-1–241103-5, Dec. 2015.

[28] Q. Li *et al.*, "Simulating the spiking response of VCSEL-based optical spiking neuron," *Opt. Commun.*, vol. 407, pp. 327–332, Jan. 2018.

[29] B. Garbin, A. Dolcemascolo, F. Prati, J. Javaloyes, G. Tissoni, and S. Barland, "Refractory period of an excitable semiconductor laser with optical injection," *Phys. Rev. E, Stat. Phys. Plasmas Fluids Relat. Interdiscip. Top.*, vol. 95, no. 1, pp. 012214-1–012214-8, Jan. 2017.

[30] S. Xiang, A. Wen, and W. Pan, "Emulation of spiking response and spiking frequency property in VCSEL-based photonic neuron," *IEEE Photon. J.*, vol. 8, no. 5, Oct. 2016, Art. no. 1504109.

[31] S. Y. Xiang *et al.*, "Cascadable neuron-like spiking dynamics in coupled VCSELs subject to orthogonally polarized optical pulse injection," *IEEE J. Sel. Top. Quantum Electron.*, vol. 23, no. 6, Nov./Dec. 2017, Art. no. 1700207.

[32] E. M. Izhikevich, "Which model to use for cortical spiking neurons?" *IEEE Trans. Neural Netw.*, vol. 15, no. 5, pp. 1063–1070, Sep. 2004.

[33] E. M. Izhikevich, "Neural excitability, spiking and bursting," *J. Bifurcation Chaos*, vol. 10, no. 6, pp. 1171–1266, 2000.
[34] E. Kandel, J. Schwartz, T. Jessell, S. Siegelbaum, and A. J. Hudspeth, *Principles of Neural Science*. New York, NY, USA: McGraw-Hill, 2000.
[35] R. Toole *et al.*, "Photonic implementation of spike-timing-dependent plasticity and learning algorithms of biological neural systems," *J. Lightw. Technol.*, vol. 34, no. 2, pp. 470–476, Jan. 15, 2016.
[36] J. Robertson, T. Deng, J. Javaloyes, and A. Hurtado, "Controlled inhibition of spiking dynamics in VCSELs for neuromorphic photonics: Theory and experiments," *Opt. Lett.*, vol. 42, no. 8, pp. 1560–1563, Apr. 2017.
[37] B. Kelleher, C. Bonatto, P. Skoda, S. P. Hegarty, and G. Huyet, "Excitation regeneration in delay-coupled oscillators," *Phys. Rev. E, Stat. Phys. Plasmas Fluids Relat. Interdiscip. Top.*, vol. 81, no. 3, p. 036204, 2010.
[38] T. Van Vaerenbergh, K. Alexander, J. Dambre, and P. Bienstman, "Excitation transfer between optically injected microdisk lasers," *Opt. Express*, vol. 21, no. 23, pp. 28922–28932, Nov. 2013.
[39] T. Van Vaerenbergh *et al.*, "Cascadable excitability in microrings," *Opt. Express*, vol. 20, no. 18, pp. 20292–20308, Aug. 2012.
[40] T. Deng, J. Robertson, and A. Hurtado, "Controlled propagation of spiking dynamics in vertical-cavity surface-emitting lasers: Towards neuromorphic photonic network," *IEEE J. Sel. Top. Quantum Electron.*, vol. 23, no. 6, Nov./Dec. 2017, Art. no. 1800408.
[41] R. Al-Seyab, K. Schires, N. A. Khan, A. Hurtado, I. D. Henning, and M. J. Adams, "Dynamics of polarized optical injection in 1550-nm VCSELs: Theory and experiments," *IEEE J. Sel. Top. Quantum Electron.*, vol. 17, no. 5, pp. 1242–1249, Sep. 2011.
[42] P. Pérez, A. Valle, I. Noriega, and L. Pesquera, "Measurement of the intrinsic parameters of single-mode VCSELs," *J. Lightw. Technol.*, vol. 32, no. 8, pp. 1601–1607, Apr. 15, 2014.

TAO DENG was born in Sichuan, China, in 1982. He received the B.Sc. degree in electronic information engineering and the M.Sc. degree in optics from Southwest University, Chongqing, China, in 2002 and 2005, respectively, and the Ph.D. degree in optics from Sichuan University, Chengdu, China, in 2012.

He is currently a Professor with the School of Physical Science and Technology, Southwest University, Chongqing. He has authored or co-authored over 30 publications. His current research mainly focuses on the nonlinear dynamics of semiconductor lasers and their applications in chaos secret communication, microwave photonics, and photonic neuron.

JOSHUA ROBERTSON was born in Glasgow, U.K., in 1994. He is currently pursuing the Ph.D. degree in physics from the University of Strathclyde, Glasgow, U.K.

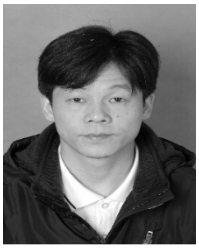

ZHENG-MAO WU was born in Wuyuan, China, in 1970. He received the B.Sc., M.Sc., and Ph.D. degrees in optics from Sichuan University, Chengdu, China, in 1992, 1995, and 2003, respectively.

He is currently a Full Professor with the School of Physical Science and Technology, Southwest University, Chongqing, China. He has authored or co-authored over 100 publications. His current research interests include nonlinear dynamics of semiconductor lasers and their applications, and chaotic semiconductor lasers and their applications.

GUANG-QIONG XIA was born in Fushun, China, in 1970. She received the B.Sc., M.Sc., and Ph.D. degrees in optics from Sichuan University, Chengdu, China, in 1992, 1995, and 2002, respectively.

She is currently a Full Professor with the School of Physical Science and Technology, Southwest University, Chongqing, China. She has authored or co-authored over 140 publications, including about 100 journal papers. Her current research interests include nonlinear dynamics of semiconductor lasers, synchronization and control of chaotic semiconductor lasers, chaos secure communication based on semiconductor lasers, and microwave photonics.

XIAO-DONG LIN was born in Chongqing, China, in 1975. He received the B.Sc., M.Sc., and Ph.D. degrees in optics from Sichuan University, Chengdu, China, in 1998, 2002, and 2012, respectively.

He is currently an Associate Professor with the School of Physical Science and Technology, Southwest University, Chongqing, China. His current researches include nonlinear dynamics of semiconductor lasers and microwave photonics.

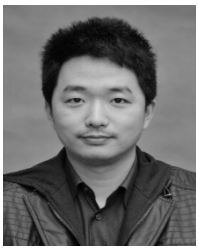

XI TANG was born in Chongqing, China, in 1982. He received the M.Sc. degree in optics from Southwest University, Chongqing, in 2009, where he is currently pursuing the Ph.D. degree in optics. His research direction mainly focuses random number generation based on chaotic semiconductor lasers.

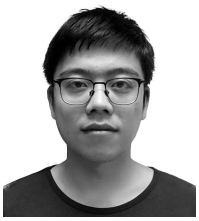

ZHI-JING WANG was born in Qiandongnan, China, in 1994. He received the B.Sc. degree in physics from Dalian Minzu University, Dalian, China, in 2016. He is currently pursuing the M.Sc. degree in optics with Southwest University, Chongqing, China.

ANTONIO HURTADO received the Ph.D. degree from the Universidad Politécnica de Madrid (UPM), Spain, in 2006. He has over 10 years of international research experience in photonics at the University of Essex, U.K., the University of Strathclyde, U.K., the University of New Mexico, USA, and UPM, Spain. In 2014, he received the Chancellor's Fellowship from the University of Strathclyde, following which he was appointed as Lecturer at the Strathclyde's Institute of Photonics. He has been a recipient of two prestigious and highly competitive Marie Curie Fellowships by the European Commission: Projects ISLAS (2009–2011) & NINFA (2011–2014).